Tetracycline hydrochloride (TCH)-loaded drug carrier based on PLA: PCL nanofibre mats: experimental characterisation and release kinetics modelling

Hazim J. Haroosh [1], Yu Dong [2,*], Kin-Tak Lau [3]

[1]*Department of Chemical Engineering, Curtin University, GPO Box U1987, Perth, WA 6845, Australia*

[2] *Department of Mechanical Engineering, Curtin University, GPO Box U1987, Perth, WA 6845, Australia*

[3]*Department of Mechanical Engineering, The Hong Kong Polytechnic University, Hung Hom, Kowloon, Hong Kong, China*

* Author to whom correspondence should be addressed.
E-mail: Y.Dong@curtin.edu.au (Y. Dong)

H. J. Haroosh
E-mail: hazim_eng@yahoo.com

K. T. Lau
E-mail: mmktlau@polyu.edu.hk

Abstract

The experimental characterisation of electrospun poly(lactic acid) (PLA): poly(ε-caprolactone) (PCL) as drug carriers, at five blend ratios from 1:0, 3:1, 1:1, 1:3 and 0:1, was holistically investigated in terms of their morphological structures, crystallinity levels and thermal properties. A widely used antibiotic tetracycline hydrochloride (TCH) was loaded to prepared fibrous mats at TCH concentrations of 1 and 5 wt%. The additional TCH into PLA: PCL better facilitates the reduction of fibre diameter than polymer blends. Increasing the TCH concentration from 1 to 5 wt% was found to result in only a modest decrease in the crystallinity level, but a significant increase in the crystallisation temperature (T_c) for PLA within PLA: PCL blends. The infrared spectra of fibre mats confirm the successful TCH encapsulation into fibrous networks. The first order and Zeng models for drug release kinetics were in better agreement with experimental release data, indicating the release acceleration of TCH with increasing its concentration. In a typical case of PLA: PCL (1:1) loaded with 5 wt% TCH, the fibre mats apparently demonstrate more wrinkled and floppy structures and increased fibre diameters and decreased inter-fibrous spaces after 7-day in vitro fibre degradation, as opposed to those obtained after 3-h degradation.

Keywords: fibre technology; characterization methods; modelling

Introduction

With a rapid growth in nanotechnology and nanomaterials ranging from health science and engineering, electrospinning becomes an efficient and versatile processing method to produce continuous ultrafine fibres on micro/nanoscaled level from prepared polymer solution with cost-competitiveness [1-8]. Its application in drug release system is of particular interest with several advantages over other dosage methods. These include the

easy incorporation of therapeutic compounds into electrospun polymer fibre carriers, well-tailored release profile by controlling the morphology, porosity and compositions of nanofibrous structures [9, 10], as well as more efficient drug release and mass transfer due to small fibre diameter, high surface areas and porous structures [11, 12].

Thakur et al. [13] successfully fabricated dual drug release electrospun scaffolds, consisting of lidocaine and mupirocin, from a poly-L-lactic acid (PLLA) solution. The release kinetics was found to be altered by at least one drug and dual spinneret technique was confirmed to be the preferred fabrication method for prototyping wound healing device. Meng et al. [14] studied both aligned and randomly oriented poly(D,L-lactide-co-glycolide) (PLGA)/chitosan nanofibrous scaffolds to release model drug fenbufen (FBF). With increasing the chitosan content, the drug release rate also increased due to the enhancement of hydrophilicity of PLGA/chitosan composite scaffolds. The nanofibre arrangement was shown to impact the release behaviour with the lower release rate taking place in aligned nanofibrous structures as opposed to randomly oriented counterparts. Katti et al. [15] initially optimised the electrospinning parameters such as needle diameter, polymer solution concentration and voltage per unit length to understand their effects on the morphology and diameter of poly(lactide-*co*-glycolide) (PLAGA) nanofibres. At the later stage, a broad-spectrum antibiotic cefazolin was used, which shows that PLAGA nanofibre scaffolds could be a potential carrier for effective antibiotic delivery systems targeting the wound treatments. Luong-Van et al. [16] showcased the use of electrospun poly(ε-caprolactone) (PCL) as a promising carrier candidate for heparin delivery to the site of vascular injury. This study found that about the half of the encapsulated heparin was released by diffusional control from electrospun heparin/PCL fibres after 14 days. There was no inflammatory response induced from such fibres in macrophage cells in vitro.

Additionally, the proliferation of vascular smooth muscle cell (VSMC) in culture was effectively prevented by heparin. Kenawy et al. [17] evaluated electrospun fibres based on PCL as a biodegradable polymer and polyurethane (PU) as a non-biodegradable polymer to deliver the anti-inflammatory drug ketoprofen. Their results indicate that the similar release rates were detected irrespective of used polymer or blend types. Nonetheless, PCL/PU blends demonstrated improved visual mechanical properties. Taepaiboon et al. [18] developed electrospun poly(vinyl alcohol) (PVA) fibre mats as drug carriers for transdermal drug delivery system. Four types of non-steroidal anti-inflammatory drug with varying water solubility property, i.e. sodium salicylate (freely soluble in water), diclofenac sodium (sparingly soluble in water), naproxen (NAP), and indomethacin (IND) (both insoluble in water), were selected as model drugs. Both release rate and total amount of released drugs from PVA fibre mats were found to be dependent upon the molecular weight of the model drugs. Increasing molecular weight of drugs appeared to decrease both the rate of total release amount. Besides, in comparison to drug-loaded as-cast films, PVA mats presented much better release characteristic.

PLA can be either semicrystalline or amorphous biopolymers, depending on the relative ratio of PLA backbone chains produced in the chemical synthesis. Its attractive material features consist of easy processability with the ability to be dissolved in common solvents [19], as well as good environmental sustainability and biocompatibility [20]. Nonetheless, PLA biodegradation can be harmful to local tissues [21] owing to its low pH value [22]. On the other hand, PCL, as a hydrophobic and semi-crystalline polymer [17], possesses a crystallisable rubbery behaviour used for the enhancement of elasticity [23]. Moreover, PCL is also well-known for its acceptable drug permeability and effective biocompatibility [24]. The PCL degradation cannot form a local acidic environment, which as the main

advantage along with its moderately low cost allows PCL to be a good polymer candidate for biomedical applications [16, 17]. In comparison, PCL often undergoes much slow degradation process and appears to be less harmful to local tissues as opposed to PLA [24].

Polymer blending represents a very essential polymer processing technique in order to develop or adjust the physicochemical properties of polymeric materials for the benefit of using mutual material merits [25]. Sometimes, generated polymer blends present totally different or unique properties from those of individual virgin polymers [26]. The simplicity of blend preparation enables to achieve greatly improved material properties by appropriate combination of basic polymeric components [27].

Nowadays, the use of biopolymers as a carrier for drug delivery systems has gained the great popularity due to promoted healing effectiveness and decrease in medical side-effects resulting from their non-toxicity [28]. Therapeutic drugs can be easily loaded into polymer fibre mats by means of electrospinning technique. The composition and morphological structures of such mats, as altered by the appropriate material fabrication, have remarkable impact on the drug release control [24]. Tetracycline hydrochloride (TCH) is a hydrophilic antibiotic used for the healing and avoidance of bacterial infections taking place in the burns, cuts and surgeries for various wound healing purposes.

The objective of this study is to evaluate the effect of PLA: PCL blend ratio on the fabrication, structural analysis and material characterisation of TCH loaded PLA: PCL fibre mats, and further to produce a new carrier system for the effective drug delivery. The mathematical modelling for drug release kinetics has also been implemented in good accordance with the experimental release data.

Experimental details

Materials

PLA 3051D pellets with the molecular weight of 93,500 g/mol was supplied by NatureWorks, USA. As-received PCL with the molecular weight of 80,000 g/mol, TCH ($C_{22}H_{24}N_2O_8 \cdot HCl$ and molecular weight of 480.9 g/mol), phosphate buffer solution (PBS), chloroform and methanol solvents were purchased from Sigma-Aldrich Ltd, Australia.

Material Fabrication via Electrospinning

Prior to the electrospinning process, 8 wt%/v PLA was initially mixed with 9 wt%/v PCL at five different blend ratios of 1:0, 3:1, 1:1, 1:3 and 0:1 by using chloroform and methanol solvents (2:1 volume ratio). Subsequently, 1 and 5 wt% TCH drugs were dissolved in methanol and further added to PLA: PCL blend solutions, respectively. Those prepared solutions were separately transferred to a medically used 10 ml plastic syringe that were mounted on a Fusion 100 syringe pump (Chemyx Inc, Stafford, TX USA), and also attached to a metallic needle with an inner diameter of 0.584 mm. The whole electrospinning process was carried out with a solution flow rate of 2 ml/h and high voltage settings between 25-28 kV at 24ºC. A mesh ground collector covered with aluminium foils was employed at a needle-to-collector distance of 13 cm to receive the electrospun fibre mats. The thickness of fibre mats were measured in range of 300-450 μm by a micrometer.

In Vitro Drug Release Study

The TCH loaded fibre mats were cut in size of 2 cm × 2 cm and underwent a rotary shaker incubation (rotor speed: 100 rpm) at 37°C at a 20 ml PBS with pH=7.4.When the required incubation time is reached for the designated drug release, the mat sample was further transferred to a 20 ml fresh buffer solution. About 11 incubations for each TCH

concentration were made for obtaining the drug release data from prepared fibre mats. Each incubation process was subjected to three repeated tests for data reproducibility. After this step, the released TCH amount in the buffer solution was determined accordingly.

In Vitro Biodegradation Study

The fibre mats with the same size were measured with the initial mass *m* and transferred to a 15 ml PBS (pH=7.4). They were subsequently subjected to the rotary shaker incubation at a rotor speed of 100 rpm in a 15 ml PBS (pH=7.4) for the biodegradation study. The fibre mats were removed at each given incubation period and further washed in deionised water. A final mass m_1 of fibre mats were obtained after drying them under vacuum at 37°C. The total mass loss *m%* was determined accordingly in a simple expression below

$$m(\%) = \left(\frac{m - m_1}{m} \right) \times 100\% \qquad (1)$$

Material Characterisation

Two critical parameters of solution viscosity and electrical conductivity in electrospinning were measured with the aid of a Visco 88 portable viscometer, Malvern Instruments, UK and a WP-81 Waterproof Conductivity Meter, TPS, Australia, respectively.

The fibre morphology was investigated by means of an EVO 40XVP scanning electron microscope (SEM), Germany at an accelerating voltage of 5 kV. Fibre mat samples were subjected to sputter coating with platinum prior to the SEM evaluation. The embedded Zeiss smart SEM software was utilised for the on-screen measurements of individual fibre diameters. The average fibre diameters were calculated based on sample measurements

from a minimum 150 fibres in multiple-scanned SEM images (i.e. at a rate of over 15 fibres per image).

Wide angle X-ray diffraction (WRD) analysis was undertaken by using a Bruker Discover 8 X-ray diffractometer, Germany, which was in operation at 40kV and 40 mA. The Cu-Kα radiation (wave length λ=1.54 Å for a Cu target) was monochromatised with graphite sample monochromators in a 2θ range from 7.5° to 40° with a scanning rate of 0.016-0.02°/s. The crystallinity level was determined by applying the area integration method [29, 30] to XRD intensity data over the range of 2θ from 8° to 27°.

Thermal analysis based on differential scanning calorimetry (DSC) was carried out using a DSC6000 Perkin Elmer, USA with a cryofill liquid nitrogen cooling system. About a 10 mg fibre mat was sealed in an aluminium crucible and subsequently underwent heating-cooling cycles from -90°C to 200°C with a ramp rate of 10°C/min. The DSC thermograms and associated thermal parameters such as glass transition temperature (T_g), crystallisation temperature (T_c) as well as melting temperature (T_m) were obtained from the first heating scan.

Fourier transform infrared spectroscopy (FTIR) was performed in a Spectrum 100 FTIR Spectrometer Perkin Elmer, Japan. The resulting spectra were captured from 4000-550 cm^{-1} with 4 cm^{-1} resolution on the basis of an attenuated total reflectance (ATR) technique [31].

The TCH amount in the PBS for in vitro drug release study was determined from a UV-vis spectrophotometer Jasco V-67, USA at a wavelength of 360 nm. The drug release curves against the release time were acquired for understanding the release kinetics of TCH from prepared fibre mats.

Mathematical Models for Drug Release Kinetics

The drug release experimental data can be fitted to some release kinetic models [32, 33] not only to assess the transport of drug molecules but also to facilitate the understanding of drug-carrier interaction whose mechanism can dictate the final drug release profile [24]. As a result, such direct interaction may lower the drug solubility, and thus retard their release from carriers [34]. This study focuses on five generally used kinetic models to interpret the drug release mechanism, namely zero order, first order, Higuchi, Ritger-Peppas and Zeng models [32-34] as detailed in the following subsections.

Zero Order Model

The zero order model is employed to a drug delivery system in which the drug release rate is independent of drug concentration. Its empirical equation [35] can be described as

$$\frac{M_t}{M_\infty} = K_0 t \qquad (2)$$

where M_t, M_∞ and K_0 are the absolute cumulative amount by mass of drug released at time t and infinite time, and the zero order release constant, respectively. The ratio M_t/ M_∞ is denoted as the cumulative release amount in percentage [32].

Apparently, M_t/ M_∞ is linearly proportional to the time t for zero order kinetics, which is an ideal method to achieve a prolonged pharmacological action. Zero order model can be implemented in the determination of drug dissolution from a widespread range of modified release dosage forms including matrix, tablet with low soluble dugs, coated tablets and capsules, as well as osmotic systems [36, 37].

First Order Model

The first order model kinetics was initially employed by Gibaldi and Feldman [38] in 1967 and later by Wagner [39] in 1969. The release in the drug delivery system is usually concentration dependent. The first order equation can be in a derived mathematical form [33, 40] for the released drug in an aqueous phase [31] below

$$\frac{M_t}{M_\infty} = 1 - e^{K_1 t} \qquad (3)$$

in which K_1 is the first order release constant.

Higuchi Model

Higuchi developed important mathematical models to study the release of water soluble and low soluble drugs loaded in semi-solid and solid matrices [41, 42]. The initial attempt was based on the validity of Higuchi model only for a planar system, which subsequently considered different geometries and matrix characteristics even for the porous structures [42-46]. The equation of Higuchi model [33, 40, 47] can be simplified as

$$\frac{M_t}{M_\infty} = K_H t^{\frac{1}{2}} \qquad (4)$$

where K_H is the Higuchi kinetic constant that reflects the design variables in the drug delivery system. In Higuchi model, the fraction of drug released is proportional to the square root of time. Higuchi model is often used under the following assumptions [47]: (i) much higher initial drug concentration than the solubility of the drug in the system, (ii) one-dimensional drug diffusion with the negligibility of edge effects, (iii) Fine state of suspended drug in which the particle diameter is much smaller than the thickness of the

system, (iv) Ignored dissolution and swelling of drug carrier, (v) Constant drug diffusivity and (vi) maintained perfect sink conditions.

Ritger-Peppas Model

Ritger and Peppas established a simple exponential relation to investigate both Fickian and non-Fickian drug release in swelling and non-swelling polymeric delivery systems [35, 48]. Such mathematical equation for Ritger-Peppas model is given by

$$\frac{M_t}{M_\infty} = K_R t^n \qquad (5)$$

Where K_R is the Ritger-Peppas kinetic constant that incorporates structural and geometric characteristics of the macromolecular network system and the drug. n is the diffusion exponent indicating the transport mechanism through the polymer. Base on different ranges of n values in Ritger-Peppas model, the drug release can be classified as Fickian diffusion release from non-swellable matrix ($n \leq 0.5$), as well as non-Fickian release in both diffusion and erosion controlled mechanisms ($0.5 < n < 1$) [35, 48]. Clearly when $n=1$, the simplified equation from Ritger-Peppas model becomes that of first order model in a special case.

Zeng Model

Zeng and co-workers recently developed a three-parameter model with the close-form analytical solution to consider the reversible drug-carrier interaction and first order drug release from liposomes [34]. The equation for Zeng model is relatively complex as given by

$$\frac{M_t}{M_\infty} = \frac{K_{off}}{K_{on} + K_{off}}\left(1 - e^{-K_S t}\right) + \frac{K_{on}}{K_{on} + K_{off}}\left(1 - e^{-K_{off} t}\right) \qquad (6)$$

and

$$\Delta G = -k_B T\left(\frac{K_{on}}{K_{off}}\right) \qquad (7)$$

In equation (6), K_{on} is the rate constant of association for non-dispersed drug molecules in the system that need to be disassociated from carriers prior to release. Conversely, K_{off} is the rate constant of disassociation accordingly and K_S is a constant proportional to the surface-to-volume ratio of carriers for the enhancement of drug release. In addition, ΔG is the free energy difference between the free and bound state, k_B is the Boltzmann's constant and T is the absolute temperature that is assumed to be 300 K in equation (7). K_{off}, K_S and ΔG are three critical parameters in Zeng model to describe the effect of cumulative drug release.

Results and Discussion

Effect of Blend Ratios and Loaded Drug on Fibre Morphology

As illustrated in Figs. 1 and 2, electrospun fibres produced from dissolved PLA in chloroform and methanol have the average fibre diameter of 510 nm. In such PLA based system, when increasing the ratio of PLA to PCL up to 3:1, a relatively large fibre diameter at 562 nm was achieved with the intermediate quality due to the non-uniform morphology, Fig. 1b. A further amount increase of PCL to 1:1 led to more uniform fibre structure with an average diameter of 689 nm. Such increasing trend for the fibre diameter continued when the ratio of PLA to PCL became (1:3) and (0:1), resulting in the fibre diameter of 742 and 786 nm, respectively. Fig. 3 illustrates the measured viscosities of different PLA: PCL blends. It has been found that viscosities of blend solutions significantly increase from 68 (PLA solution only) to 138 cP in a linearly monotonic manner by increasing the quantity of

PCL in the PLA: PCL system. The PCL solution offers the highest viscosity of 182 cP among all the prepared solutions. According to our previous work [3], fibre diameter is dominantly influenced by the solution viscosity. As is well understood, in viscous solutions, there are a greater number of entanglements per polymer chain which is a prerequisite for the formation of a stable jet, and this phenomenon also compensates for the detrimental effect of increased surface tension, resulting in the jet shrinkage [49].

On the other hand, the loaded 1 and 5 wt% TCH drug into PLA: PCL (1:1) system further reduce the fibre diameter to 364 and 302 nm, respectively, Fig. 2. This result can be attributed to the remarkable enhancement of electrical conductivity from 31 to 90 μs/cm when the TCH concentration increases from 1 to 5 wt%, as opposed to 1 μs/cm for the solution without TCH, Table 1. The increase of electrical conductivity inevitably produces more electric charges that are carried by the electrospinning jet so that resulting fibres can be further elongated with smaller diameter [50, 51]. Moreover, the replacement of partial polymers of either PLA or PCL (with far higher molecular weights) by very low molecular weight TCH inevitably decreases the solution viscosity, thus resulting in the smaller fibre diameters depicted in Fig. 2.

Crystallinity and Thermal Properties

The effect of the TCH concentration on the degree of crystallinity and crystalline structures of electrospun fibre samples was investigated by an XRD examination. All the blend samples demonstrate two distinct diffraction peaks at $2\theta=20.11°$ and 23.2° similar to those strong peaks from neat PCL fibres, which correspond to the crystal planes (101) and (200), respectively, Fig. 4. Their peak positions have not been greatly altered, indicating that the loaded TCH has minor impact on the crystalline structures of electrospun PLA: PCL fibres.

As a result, TCH drug is most likely to be dispersed in an amorphous state in PLA: PCL fibrous structures. Besides, the solvent evaporation may be accelerated due to the large fibre surface area and small fibre diameters generated in the electrospinning process. This phenomenon can provide a short period for the drug formation and recrystallisation of preferred configuration in amorphous state [52]. PCL fibres possess distinct high-intensity XRD peaks with a higher degree of crystallinity (X_c) about 68% whilst PLA fibres indicate dominant amorphous phases (as seen from almost invisible peaks in the inserted diagram in Fig. 4) with the X_c value of only 13%, Table 2. Even though the peak intensities for PLA: PCL blends are between those of PLA and PCL fibres, a higher PCL concentration from their blend ratio of 3:1 to 1:1 expectedly leads to the enhanced peak intensities that may contribute to the increased X_c. Irrespective of the TCH drug loading, it has been found that the X_c increases from 37% for PLA: PCL (3:1) to 43-46% for PLA: PCL (1:1).

The DSC results of electrospun PLA, PCL and PLA:PCL fibres loaded with or without TCH drug are shown in Fig. 5 and Table 2. The glass transition temperature (T_g) and melting temperature (T_m) of PCL moderately decrease when increasing the TCH concentration from 0 to 5 wt%. However, the blend ratio and the use of TCH have little impact on the T_m of PLA within polymer blends, which is in range of 151-152 ºC (but less than 157 ºC for PLA fibres). In principle, short chains of TCH molecules cause their decreased packing density, and this facilitates the chain mobility leading to the lower T_g of PCL. The loaded TCH to PLA: PCL (1:1) shows an insignificant change of crystallisation temperature (T_c) at 1 wt% concentration when compared to PLA: PCL (1:1) and PLA: PCL (3:1). At the TCH concentration of 5 wt%, T_c underwent a drastic increase at over 99 ºC as opposed to 81 ºC of PLA within PLA: PCL (1:1) and 87 ºC for PLA fibres. This result

suggests that low molecular weight TCH with a higher concentration of 5 wt% may hinder the cold crystallisation process of PLA, which plays an anti-nucleating agent role.

FTIR Evaluation

Figure 6 depicts the FTIR spectra of different material samples including TCH, PLA: PCL and PLA: PCL/TCH. Initially two carbonyl stretching (C=O) bands are assigned to 1724 cm^{-1} for PCL and 1758 cm^{-1} for PLA in electrospun PLA:PCL nanofibres; whereas the bands located at 2866 cm^{-1} (PLA component) and 2944 cm^{-1} (PCL component) are in description of C-H stretching. Furthermore, the peaks designated at 1457 and 1366 cm^{-1} specify a C-H deformation of PLA. It has also been found that many peaks representing C-C and C-O stretching are among the range from 1240 to 840 cm^{-1} for PLA and PCL. When the blend ratio of PLA: PCL increases from 1:1 to 3:1 with a higher amount of PLA, carbonyl stretching (C=O) bands at 1758 cm^{-1} for PLA become more prominent.

For TCH loaded PLA: PCL counterparts, despite the band shifting, two weak bands at 1614 and 1581 cm^{-1} have been observed for PLA: PCL (1:1) loaded with 5 wt% TCH, which are assigned to C=O stretching in ring A and C=O stretching in ring C, respectively, in good accordance with those assigned to TCH drug alone. This finding confirms the successful encapsulation of TCH into PLA: PCL blends. Such allocated bands appear to be quite vague for 1 wt% TCH loaded PLA: PCL (1:1), which is most likely to arise from the use of low TCH concentration.

In Vitro Drug Release

As mentioned earlier, a balanced level of crystallinity can be achieved in PLA: PCL (1:1) blend system since PCL with its high level of crystallinity restricts the mobility of drug molecules to make them stay around the fibre surfaces while PLA with relatively low

crystallinity can accelerate the fibre degradation. Typical TCH release profiles obtained from electrospun PLA: PCL (1:1) nanofibres loaded with 1 and 5 wt% TCH are presented in Fig. 7. Similarly, both material samples indicate the fast drug release performance. In the initial 20 mins, 44% drug was released from PLA: PCL (1:1)/ 1 wt% TCH samples in contrast with 56 % from PLA: PCL (1:1)/ 5 wt% TCH. In the first 2 h, this release increases up to 59% and 64% for 1 and 5 wt% TCH loaded samples, respectively. This drastic release step is followed by a steady release in the remaining 10-day release tests. Such a fast release is associated with the great tendency of TCH drug molecules located on the surface of electrospun fibrous structures in that the fast evaporation of solvents and high ionic interactions generally occur in the electrospinning process. The faster release of TCH, when 5 wt% TCH was added to PLA: PCL blends, can result from the moving trend of dissolved TCH to the nanofibre surface over the electrospinning period. This movement accelerates the drug release rate compared with that for a low TCH concentration at 1 wt%. Increasing the TCH concentration in PLA: PCL blends leads to a decrease of crystallinity level for PLA: PCL as shown in Table 2. Since drug release takes place initially from the amorphous regions [16], it is also plausible to assume that TCH molecules tend to accumulate in the amorphous regions in view of little changes in the crystalline structures of PLA: PCL, Fig. 4. As a result, the higher amount of TCH may result in a faster drug release rate from these regions. Our fabricated fibrous mats in this study provide a drug release profile with biomaterial and bioactive structures. They may become good carrier candidates to be employed in a range of wound healing application, as well as for the infective prevention after surgery with the requirement of fast drug release.

Release Kinetics

The release kinetics of TCH drug was investigated by fitting five aforementioned mathematical models to the release data, as illustrated in Figs. 8a and b. The obtained model parameters are summarised in Table 3. The first order and Zeng models have better agreement with the release data with higher R^2 values at 0.889 and 0.948 for 1% TCH loaded fibre mats as well as 0.930 and 0.975 for 5% TCH loaded counterparts, respectively. The better fitting with the first order model may confirm the dependent effect of drug release upon the drug concentration and used carriers. On the other hand, according to Zeng model, the diffusion process and interaction between PLA: PCL blends and TCH also have significant impact on the drug release. When the TCH concentration increases from 1 to 5 wt%, ΔG as a critical parameter also increases from 1.47×10^{-21} J to 2.49×10^{-21} J, which suggests the increase of TCH release and diffusivity owing to the greater amount of free TCH molecules on the PLA: PCL nanofibre surfaces. Furthermore, the other important parameter K_S increased from 5.127 to 8.343 h^{-1}, indicating the pore size becomes much larger when the TCH concentration increases. The variations in the fitted model parameters, especially ΔG and K_S, are consistent with the previous interpretations of the drug release results.

In Vitro Biodegradation

Due to the vague bands for 1 wt% TCH loaded PLA: PCL (1:1) in FTIR results mentioned earlier in Fig. 6, the biodegradation behaviour was characterised in Table 4, based solely on PLA: PCL nanofibres with the relatively high TCH concentration (i.e. PLA: PCL (1:1)/ 5% TCH). After the degradation in PBS for the first 3-12 h, the mass loss of nanofibre mats is quite minimal (<0.81%). When the degradation time increases up to 336 h, the mass loss

shows an insignificant increase of only 6.30%. This result can be explained partially by the semi-crystalline characteristic of PCL to preclude its degradation in a buffer solution [53]. In fact, in the absence of a biocatalyst, very little PCL degradation has been previously found in PBS [54, 55].

Figure 9 demonstrates the change of morphological structures in such nanofibre mats after being immersed in PBS over a two-week period. Nanofibres appear to be squashed to a great extent with the time, resulting in increased fibre diameters and decreased inter-fibre spaces after 7 days. More wrinkled structures have been observed after 7 days as opposed to those for the 3 h degradation. The degradation could initially take place in the amorphous region of PLA: PCL nanofibres, and then around the crystalline area [56, 57]. In case of PLA component within PLA: PCL blends, nanofibre degradation in PBS tends to be heterogeneous. The degradation of nanofibre surfaces may be slower than that in the core areas where carboxylic acid groups exist by ester hydrolysis [58]. However, the swelling of nanofibres increases since TCH molecules, prevalently located on the nanofibre surfaces according to previous in vitro drug release study, would be flushed out faster than those confined inside fibrous structures. Consequently, more buffer solution penetrates through channels generated by the released TCH, Fig. 9).

Conclusions

This investigation concentrated on the analysis of structure and morphological properties of electrospun PLA: PCL using different blend ratios and with/without the TCH drug. The fibre diameters were significantly reduced when loaded with 1 and 5 wt% TCH into PLA: PCL. The degree of crystallinity of PLA: PCL was enhanced from 37% to 46% with decreasing the blend ratio from 3:1 to 1:1 accordingly. The use of TCH loaded to PLA: PCL (1:1) offered the moderate decreases of degree of crystallinity, (T_g) and T_m of PCL by

increasing TCH concentration from 0 to 5 wt%; whereas the T_c of PLA within PLA: PCL blends increased remarkably, especially at the TCH concentration of 5 wt%, implying the anti-nucleating agent role of TCH to hinder the cold crystallisation of PLA. The infrared spectra of electrospun PLA:PCL nanofibres proved the successful encapsulation of TCH into the nanofibres. The release of TCH drug was found to be accelerated by increasing the TCH concentration. The overall fast drug release performance is manifested, which suggests its main applications for wound healing and quick surgery infective protection. In terms of understanding the release kinetics, release data were better fitted with the first order and Zeng models. Small mass loss of only 6.30% was observed at the degradation time of 336 h for PLA: PCL (1:1)/ 5 wt% TCH. However, geometric changes of degraded nanofibres such as squashed fibres with increase diameters and decreased inter-fibre spaces were clearly shown after 7 days of degradation.

References

[1] Chowdhury M, Stylios G (2011) Process optimization and alignment of PVA/$FeCl_3$ nano composite fibres by electrospinning. J Mater Sci 46: 3378-3386.

[2] Dong Y, Chaudhary D, Haroosh H, Bickford T (2011) Development and characterisation of novel electrospun polylactic acid/tubular clay nanocomposites. J Mater Sci 46: 6148-6153.

[3] Haroosh HJ, Chaudhary DS, Dong Y (2012) Electrospun PLA/PCL fibers with tubular nanoclay: morphological and structural analysis. J Appl Polym Sci 124: 3930-3939.

[4] Haroosh HJ, Dong Y, Chaudhary DS, Ingram GD, Yusa S (2013) Electrospun PLA: PCL composites embedded with unmodified and 3-aminopropyltriethoxysilane (ASP) modified halloysite nanotubes (HNT). Appl Phys A: Mater Sci Process 110: 433-442.

[5] Dong Y, Bickford T, Haroosh HJ, Lau KT, Takagi H (2013) Multi-response analysis in the material characterisation of electrospun poly (lactic acid)/ halloysite nanotube composite fibres based on Taguchi design of experiments: fibre diameter, non-intercalation and nucleation effects. Appl Phys A: Mater Sci Process 112: 747-757.

[6] Azman NN, Siddiqui S, Haroosh H, Albertran H, Johannessen B, Dong Y, Low IM (2013) Characteristics of x-ray attenuation in electrospun bismuth oxide/poly-lactic acid nanofibre mats. J Synchroton Rad 20: 741-748.

[7] Albetran H, Haroosh H, Dong Y, Prida VM, O'Connor BH, Low IM (2014) Phase transformations and crystallization kinetics in electrospun TiO_2 nanofibers in air and argon atmospheres. Appl Phys A: Mater Sci Process, in press (DOI: 10.1007/s00339-014-8246-1).

[8] Dong Y, Mosaval T, Haroosh HJ, Umer R, Takagi H, Lau KT (2014) The potential use of electrospun PLA nanofibres as alternative reinforcements in an epoxy composite system. J Polym Sci Part B: Polym Phys 52: 618-623.

[9] Kim K, Luu YK, Chang C, Fang D, Hsiao BS, Chu B, Hadjiargyrou M (2004) Incorporation and controlled release of a hydrophilic antibiotic using poly(lactide-*co*-glycolide)-based electrospun nanofibrous scaffolds. J Control Release 98: 47-56.

[10] Haroosh HJ, Dong Y, Ingram GD (2013) Synthesis, morphological structures and material characterization of electrospun PLA: PCL/magnetic nanoparticle composites for drug delivery. J Polym Sci Part B: Polym Phys 51: 1607-1617.

[11] Nair LS, Bhattacharyya S, Laurencin CT (2004) Development of novel tissue engineering scaffolds via electrospinning. Expert Opin Biol Ther 4: 659-668.

[12] Verreck G, Chun I, Rosenblatt J, Peeters J, Dijck AV, Mensch J, Noppe M, Brewster ME (2003) Incorporation of drugs in an amorphous state into electrospun nanofibers

composed of a water-insoluble, nonbiodegradable polymer. J Control Release 92: 349-360.

[13] Thakur RA, Florek CA, Kohn J, Michniak BB (2008) Electrospun nanofibrous polymeric scaffold with targeted drug release profiles for potential application as wound dressing. Int J Pharm 364: 87-93.

[14] Meng ZX, Zheng W, Li L, Zheng YF (2011) Fabrication, characterization and in vitro drug release behavior of electrospun PLGA/chitosan nanofibrous scaffold. Mater Chem Phys 125: 606-611.

[15] Katti DS, Robinson KW, Ko FK, Laurencin CT (2004) Bioresorbable nanofiber-based systems for wound healing and drug delivery: Optimization of Fabrication Parameters. J Biomed Mater Res Part B 70B: 286-296.

[16] Luong-Van E, Grøndahl L, Chua KN, Leong KW, Nurcombe V, Cool SM (2006) Controlled release of heparin from poly (ε-caprolactone) electrospun fibers. Biomaterials 27: 2042-2050.

[17] Kenawy E, Abdel-Hay F, El-Newehy M, Wnek G (2009) Processing of polymer nanofibers through electrospinning as drug delivery systems. Mater Chem Phys 113: 296-302.

[18] Taepaiboon P, Rungsardthong U, Supaphol P (2006) Drug-loaded electrospun mats of poly(vinyl alcohol) fibres and their release characteristics of four model drugs. Nanotechnology 17: 2317.

[19] Deng XL, Sui G, Zhao ML, Chen GQ, Yang XP (2007) Poly (L-lactic acid)/hydroxyapatite hybrid nanofibrous scaffolds prepared by electrospinning. J Biomater Sci-Polym Ed 18: 117-130.

[20] Lim LT, Auras R, Rubino M (2008) Processing technologies for poly (lactic acid). Progress in polymer science. Prog Polym Sci 33: 820-852.

[21] Touny A, Lawrence J, Jones A, Bhaduri S (2010) Effect of electrospinning parameters on the characterization of PLA/HNT nanocomposite fibers. J Mater Res 25: 857-865.

[22] Xu X, Zhong W, Zhou S, Trajtman A, Alfa M (2010) Electrospun PEG–PLA nanofibrous membrane for sustained release of hydrophilic antibiotics. J Appl Polym Sci 118: 588-595.

[23] Lee K, Kim H, Khil M, Ra Y, Lee D (2003) Characterization of nano-structured poly (ε-caprolactone) nonwoven mats via electrospinning. Polymer 44: 1287-1294.

[24] Huang Z, He C, Yang A, Zhang Y, Han X, Yin J, Wu Q (2006) Encapsulating drugs in biodegradable ultrafine fibers through co-axial electrospinning. J Biomed Mater Res Part A 77: 169-179.

[25] Picciani PHS, Medeiros ES, Pan Z, Orts WJ, Mattoso LHC, Soares BG (2009) Development of conducting polyaniline/poly (lactic acid) nanofibers by electrospinning. J Appl Polym Sci 112: 744-752.

[26] Islam M (2010) Fabrication and characterization of poly (vinyl alcohol)/alginate blend nanofibers by electrospinning method. Colloid Surf A-Physicochem Eng Asp 366: 135-140.

[27] Dhandayuthapani B, Krishnan U, Sethuraman S (2010) Fabrication and characterization of chitosan gelatin blend nanofibers for skin tissue engineering. J Biomed Mater Res Part B 94: 264-272.

[28] Xie Z, Buschle-Diller G (2010) Electrospun poly (D, L lactide) fibers for drug delivery: The influence of cosolvent and the mechanism of drug release. J Appl Polym Sci 115: 1-8.

[29] Alexander LE (1969) X-ray diffraction methods in polymer science. Wiley, New York.

[30] Ning N, Yin Q, Luo F, Zhang Q, Du R & Fu Q (2007) Crystallization behavior and mechanical properties of polypropylene/halloysite composites, Polymer 48: 7374-7384

[31] Chittur KK (1998) FTIR/ATR for protein adsorption to biomaterial surfaces. Biomaterials19: 357-369.

[32] Cai X, Luan Y, Dong Q, Shao W, Li Z, Zhao Z (2011) Sustained release of 5-fluorouracil by incorporation into sodium carboxymethylcellulose sub-micron fibers. Int J Pharm 419: 240-246.

[33] Das RK, Kasoju N, Bora U (2010) Encapsulation of curcumin in alginate-chitosan-pluronic composite nanoparticles for delivery to cancer cells. Nanomed-Nanotechnol Biol Med 6: 153-160.

[34] Zeng L, An L, Wu X (2011) Modeling Drug-Carrier Interaction in the Drug Release from Nanocarriers. J Drug Deliv Article ID 370308: 15 pages.

[35] Ritger PL, Peppas NA (1987) A simple equation for description of solute release I. Fickian and non-Fickian release from non-swelliable devices in the form of slabs, spheres, cylinders or discs. J Control Release 5: 23-36.

[36] Varelas CG, Dixon DG, Steiner CA (1995) Zero-order release from biphasic polymer hydrogels. Journal of Controlled Release. J Control Release 34: 185-192.

[37] Kalam MA, Humanyun M, Parvez N, Yada S, Garg A, Amin S, Sultana Y, Ali A (2007) Release kinetics of modified pharmaceutical dosage forms: A review. Continental J Pharm Sci 1: 30-35.

[38] Gibaldi M, Feldman S (1967) Establishment of sink conditions in dissolution rate determinations. Theoretical considerations and application to nondisintegrating dosage forms. J Pharm Sci 56: 1238-1242.

[39] Wagner JG (1969) Interpretation of percent dissolved-time plots derived from in vitro testing of conventional tablets and capsules. J Pharm Sci 58:1253-1257.

[40] Li P, Dai YN, Zhang JP, Wang AQ, Wei Q (2008) Chitosan-alginate nanoparticles as a novel drug delivery system for nifedipine. Int J Biomed Sci 4: 221-228.

[41] Higuchi T (1961) Rate of release of medicaments from ointment bases containing drugs in suspension. J Pharm Sci 50: 874-875.

[42] Higuchi T (1963) Mechanism of sustained-action medication.Theoretical analysis of rate of release of solid drugs dispersed in solid matrices. J Pharm Sci 52: 1145-1149.

[43] Desai SJ, Simonelli AP, Higuchi WI (1965) Investigation of factors influencing release of solid drug dispersed in inert matrices. J Pharm Sci 54: 1459-1464.

[44] Desai SJ, Singh P, Simonelli AP, Higuchi WI (1966) Investigation of factors influencing release of solid drug dispersed in inert matrices II: Quantitation of procedures. J Pharm Sci 55: 1224-1229.

[45] Lapidus H, Lordi NG (1966) Some factors affecting the release of a water-soluble drug from a compressed hydrophilic matrix. J Pharm Sci 55: 840-843.

[46] Lapidus H, Lordi NG (1968) Drug release from compress hydrophilic matrices. J Pharm Sci 57: 1292-1301.

[47] Siepmann J, Peppas NA (2001) Modeling of drug release from delivery systems based on hydroxypropylmethlcellulose (HPMC). Adv Drug Deliv Rev 48: 139-157.

[48] Ritger PL, Peppas NA (1987) A simple equation for description of solute release II. Fickian and anomalous release from swellable devices. J Control Release 5: 37-42.

[49] Spasova M, Stoilova O, Manolova N, Rashkov I, Altankov G (2007) Preparation of PLLA/PEG nanofibers by electrospinning and potential applications. J Bioact Compa Polym 22: 62-76.

[50] Lee G, Song J, Yoon K (2010) Controlled wall thickness and porosity of polymeric hollow nanofibers by coaxial electrospinning. Macromol Res 18: 571-576.

[51] Saraf A, Lozier G, Haesslein A, Kasper FK, Raphael RM, Baggett LS, Mikos AG (2009) Fabrication of Nonwoven Coaxial Fiber Meshes by Electrospinning. Tissue Eng-Part C 15: 333-344.

[52**]** Puppi D, Piras A, Detta N, Dinucci D, Chiellini F (2010) Poly (lactic-co-glycolic acid) electrospun fibrous meshes for the controlled release of retinoic acid. Acta Biomater 6: 1258-1268.

[53] Sinha VR, Bansal K, Kaushik R, Kumria R, Trehan A (2004) Poly-ε-caprolactone microspheres and nanospheres: An overview. Int J Pharm 278: 1-23.

[54] Gan ZH, Liang QZ, Zhang J, Jing XB (1997) Enzymatic degradation of poly (ε-caprolactone) film in phosphate buffer solution containing lipases. Polym Degrad Stab 56: 209-213.

[55] Pastorino L, Piolic F, Zillid M, Convertid A, Nicolini C (2004) . Lipasecatalyzed degradation of poly(ε -caprolactone). Enzyme Microb Technol 35: 321-326.

[56] Huang MH, Li S, Vert M (2004) Synthesis and degradation of PLA–PCL–PLA triblock copolymer prepared by successive polymerization of ε-caprolactone and DL-lactide. Polymer 45: 8675-8681.

[57] Stefani M, Coudane J, Vert M (2006) In vitro ageing and degradation of PEG–PLA diblock copolymer-based nanoparticles. Polym Degrad Stab 91: 2554-2559.

[58] Maquet V, Boccaccini AR, Pravata L, Notingher I, Jérôme R (2004) Porous poly(α-hydroxyacid)/Bioglass® composite scaffolds for bone tissue engineering. I: preparation and in vitro characterisation. Biomaterials 25: 4185-4194.

List of Figures

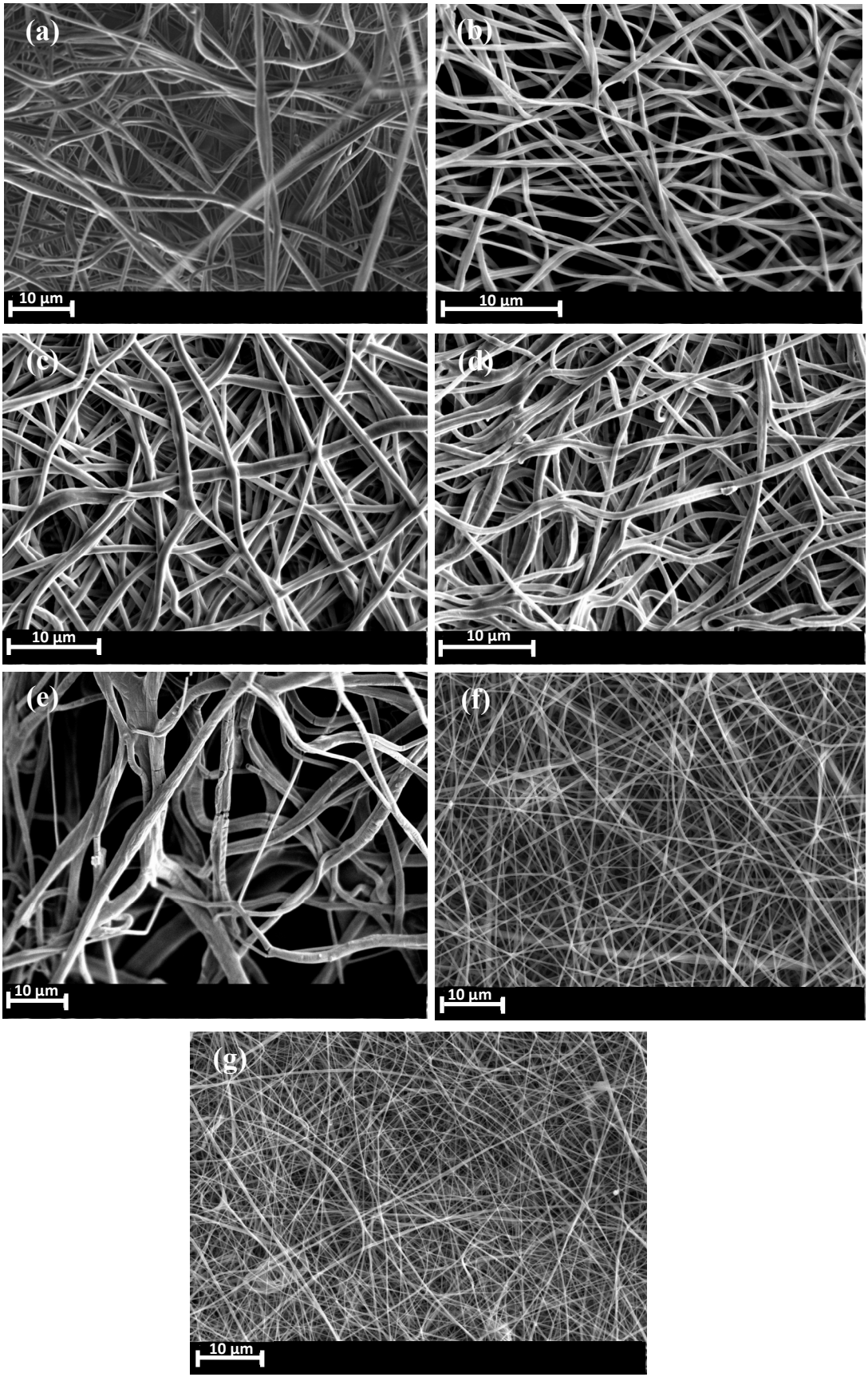

Fig. 1

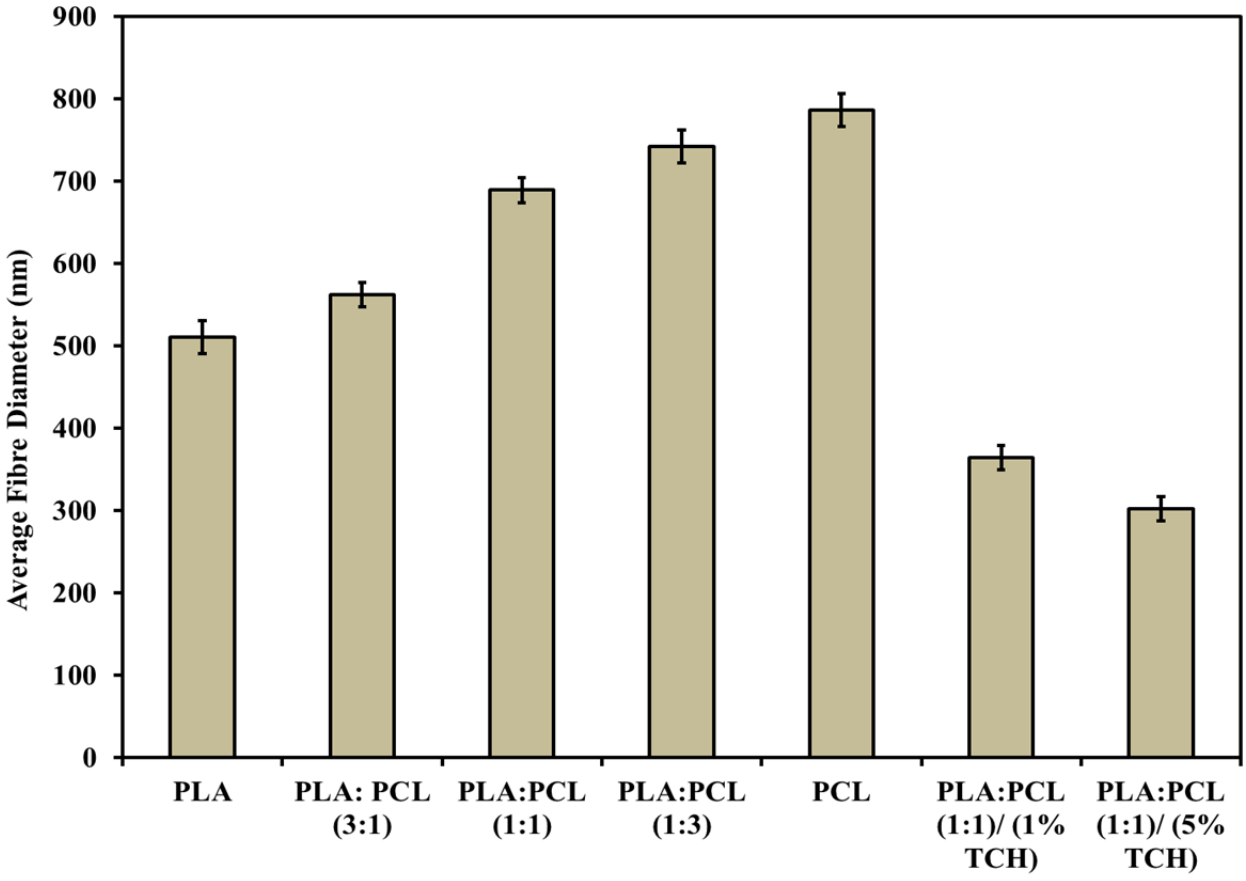
Average Fibre Diameter (nm)
900
800
700
600
500
400
300
200
100
0
PLA
PLA: PCL (3:1)
PLA:PCL (1:1)
PLA:PCL (1:3)
PCL
PLA:PCL (1:1)/ (1% TCH)
PLA:PCL (1:1)/ (5% TCH)

Fig. 2

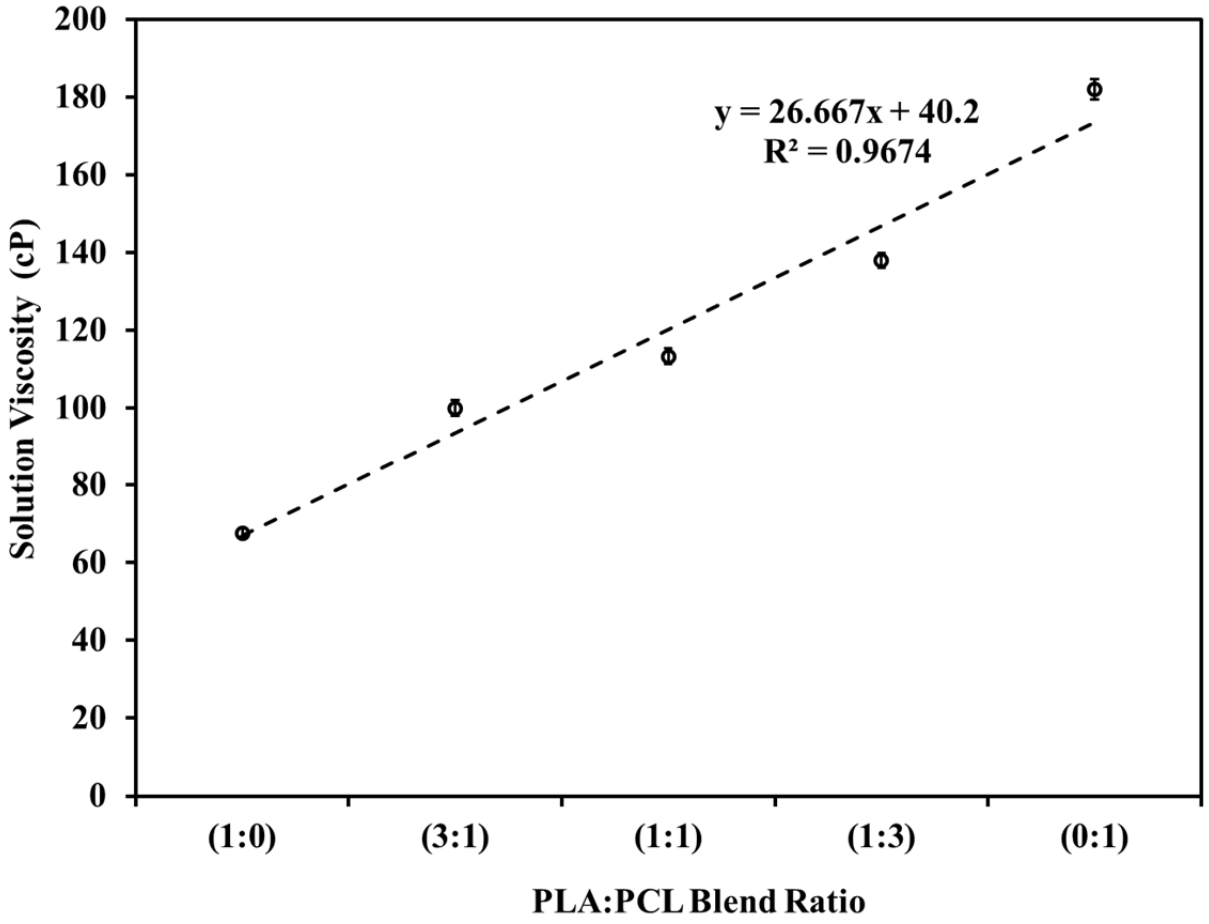
200
180
160
140
120
100
80
60
40
20
0
Solution Viscosity (cP)
y = 26.667x + 40.2
R² = 0.9674
(1:0)
(3:1)
(1:1)
(1:3)
(0:1)
PLA:PCL Blend Ratio

Fig. 3

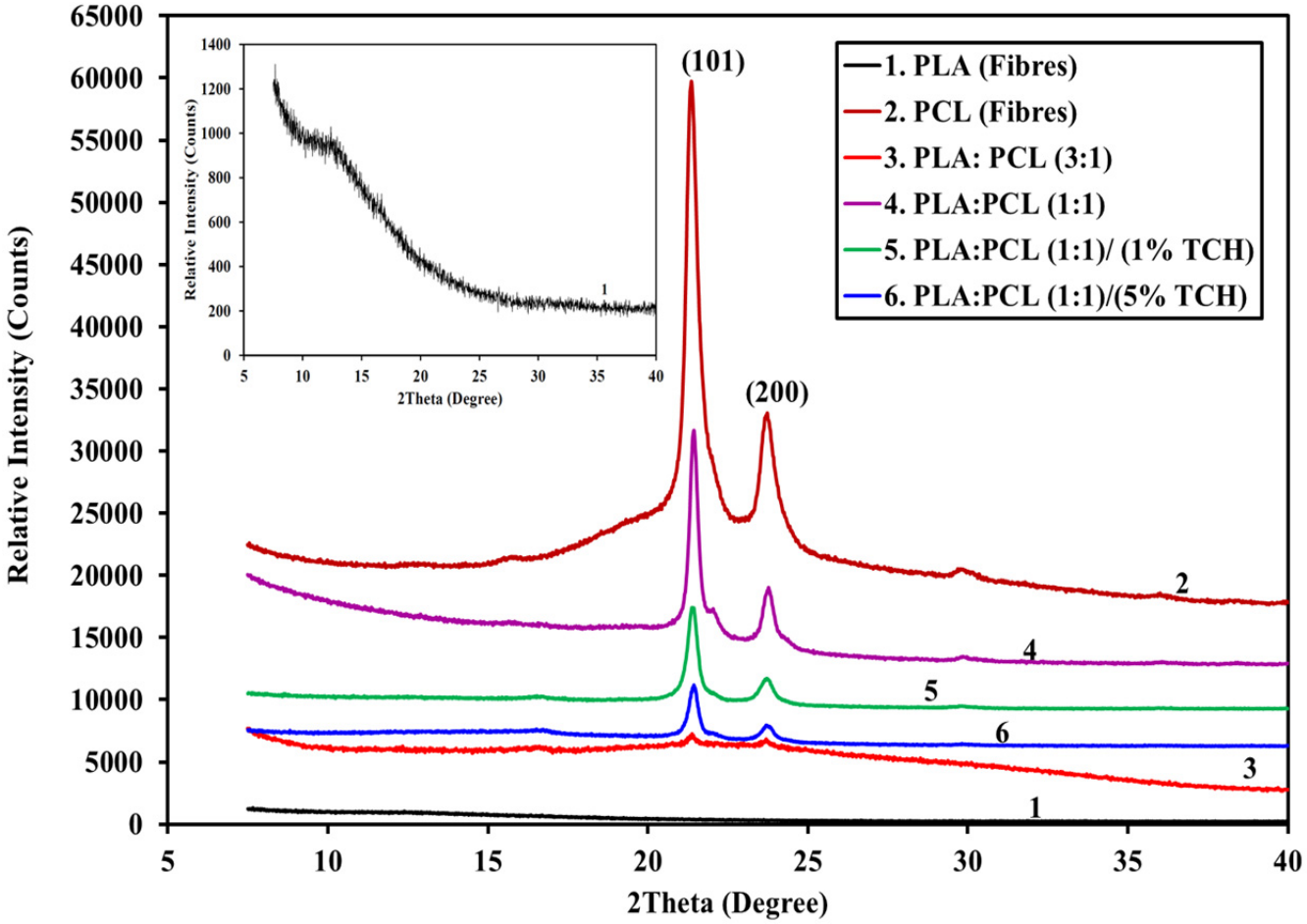
Relative Intensity (Counts)
2Theta (Degree)
(101)
(200)
1. PLA (Fibres)
2. PCL (Fibres)
3. PLA: PCL (3:1)
4. PLA:PCL (1:1)
5. PLA:PCL (1:1)/ (1% TCH)
6. PLA:PCL (1:1)/(5% TCH)
1
2
3
4
5
6

Fig. 4

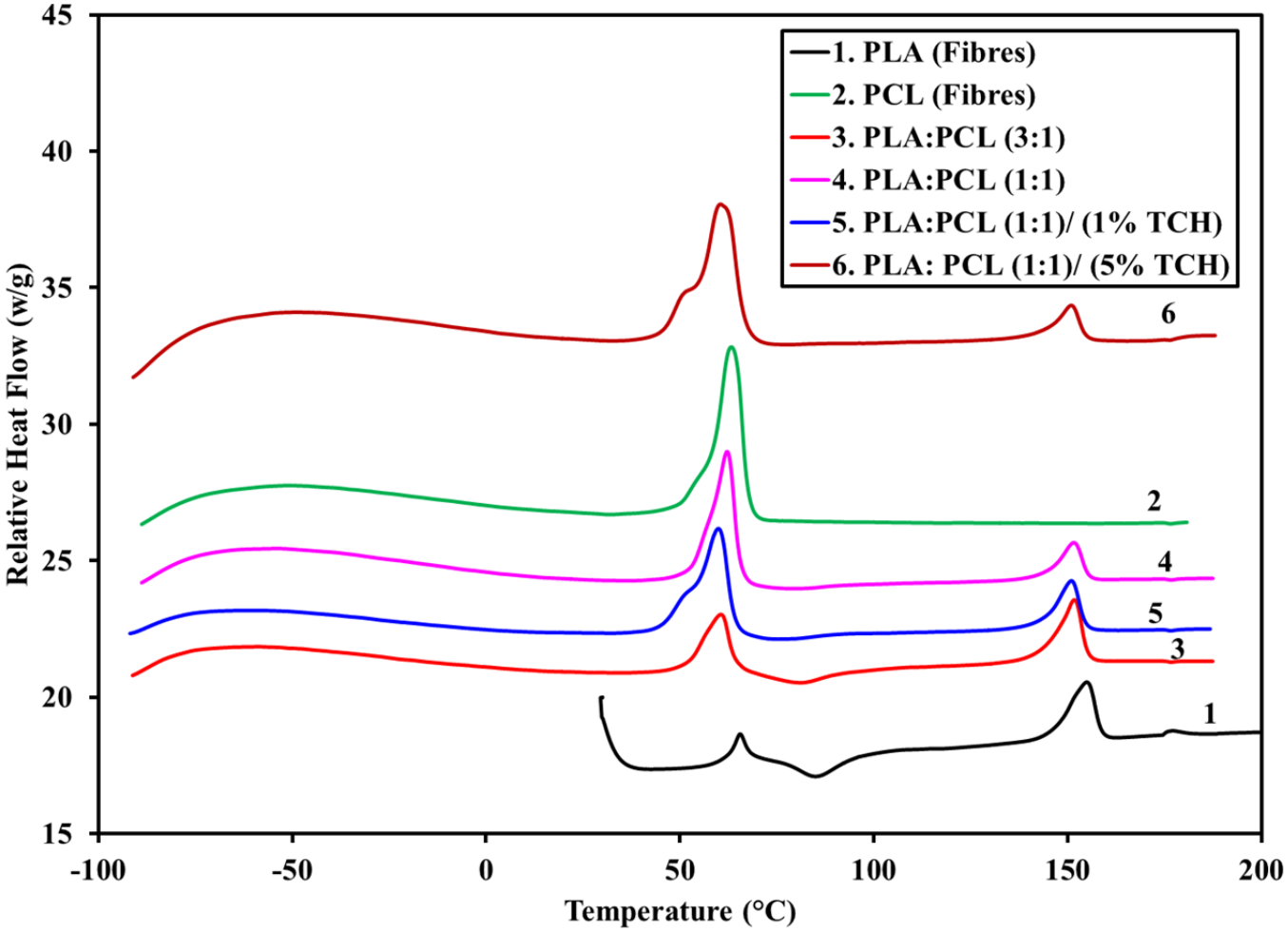
1. PLA (Fibres)
2. PCL (Fibres)
3. PLA:PCL (3:1)
4. PLA:PCL (1:1)
5. PLA:PCL (1:1)/ (1% TCH)
6. PLA: PCL (1:1)/ (5% TCH)
Relative Heat Flow (w/g)
Temperature (°C)
45
40
35
30
25
20
15
-100
-50
0
50
100
150
200
6
2
4
5
3
1

Fig. 5

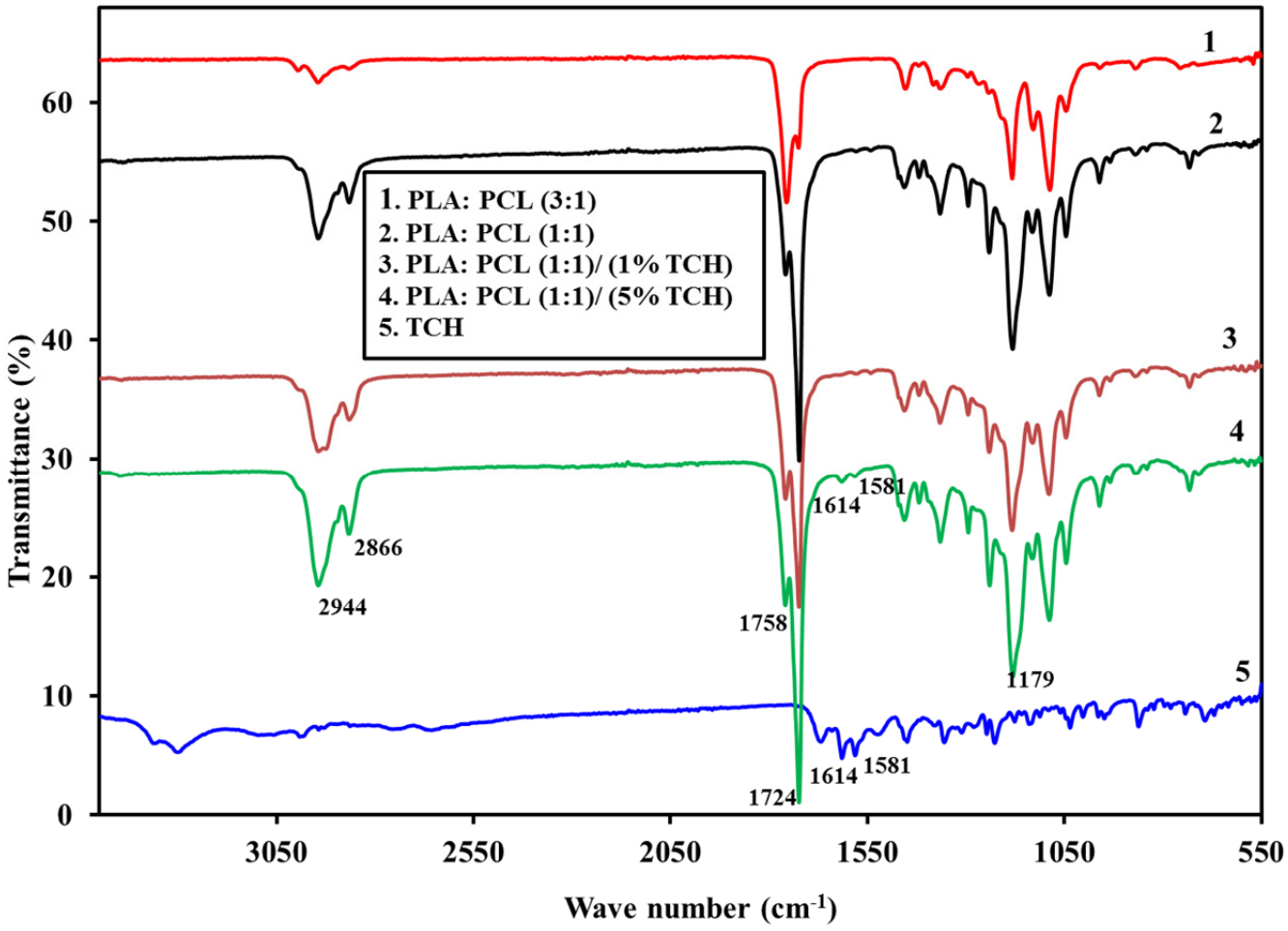
1. PLA: PCL (3:1)
2. PLA: PCL (1:1)
3. PLA: PCL (1:1)/ (1% TCH)
4. PLA: PCL (1:1)/ (5% TCH)
5. TCH
Transmittance (%)
Wave number (cm-1)
0
10
20
30
40
50
60
3050
2550
2050
1550
1050
550
1
2
3
4
5
2944
2866
1758
1724
1614
1581
1614
1581
1179

Fig. 6

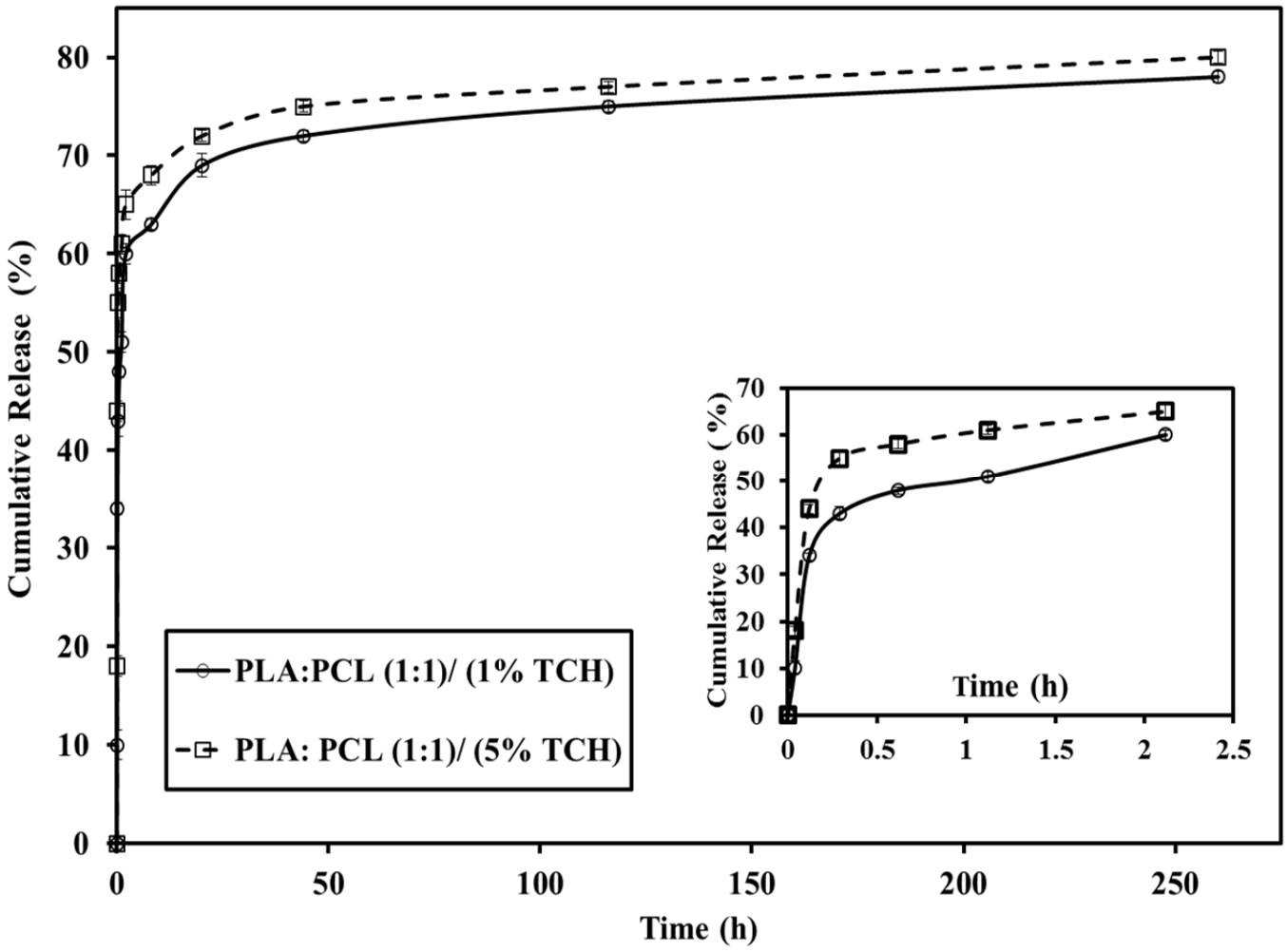
Cumulative Release (%)
Time (h)
PLA:PCL (1:1)/ (1% TCH)
PLA: PCL (1:1)/ (5% TCH)
Cumulative Release (%)
Time (h)

Fig. 7

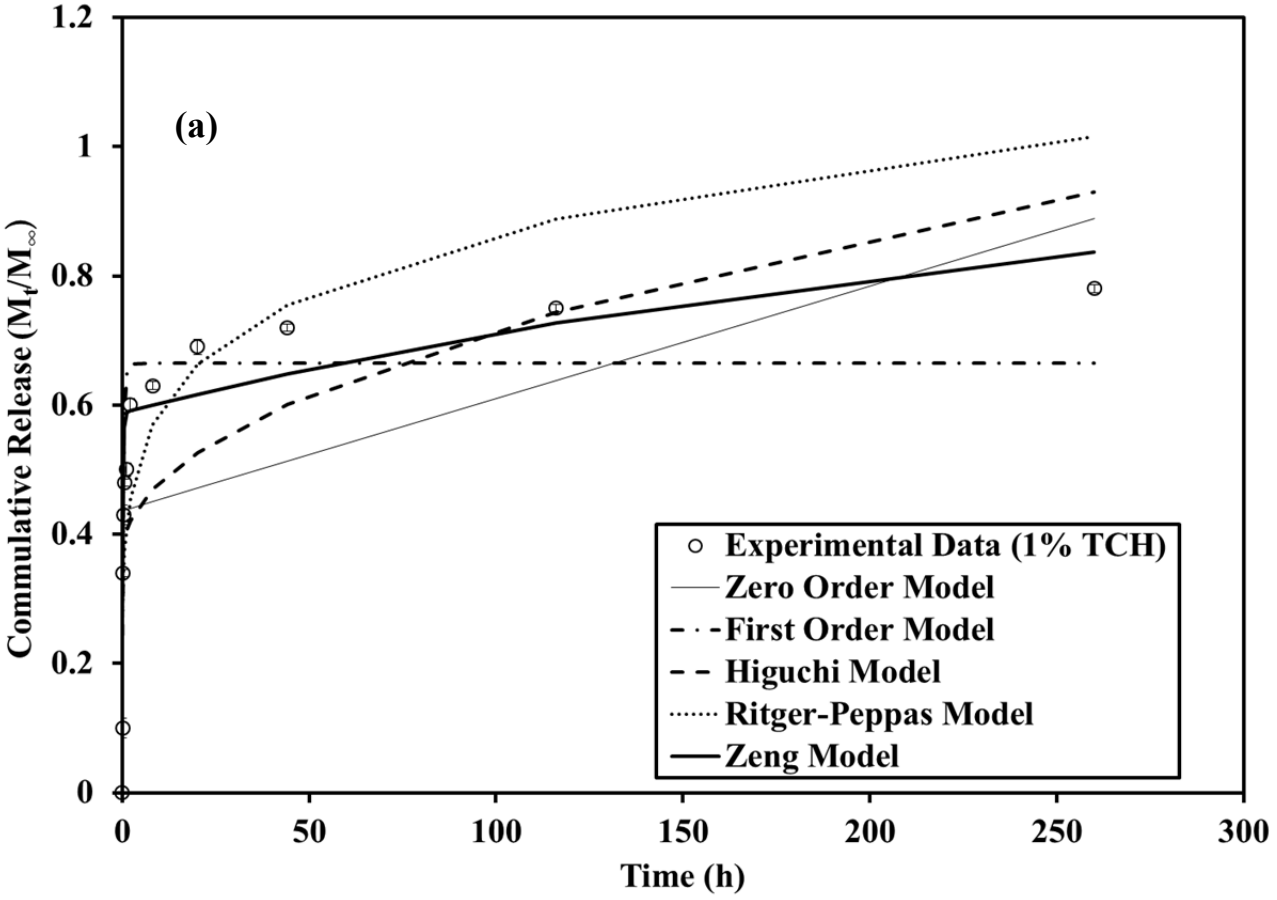
(a)
Commulative Release (M_t/M_∞)
Time (h)
Experimental Data (1% TCH)
Zero Order Model
First Order Model
Higuchi Model
Ritger-Peppas Model
Zeng Model

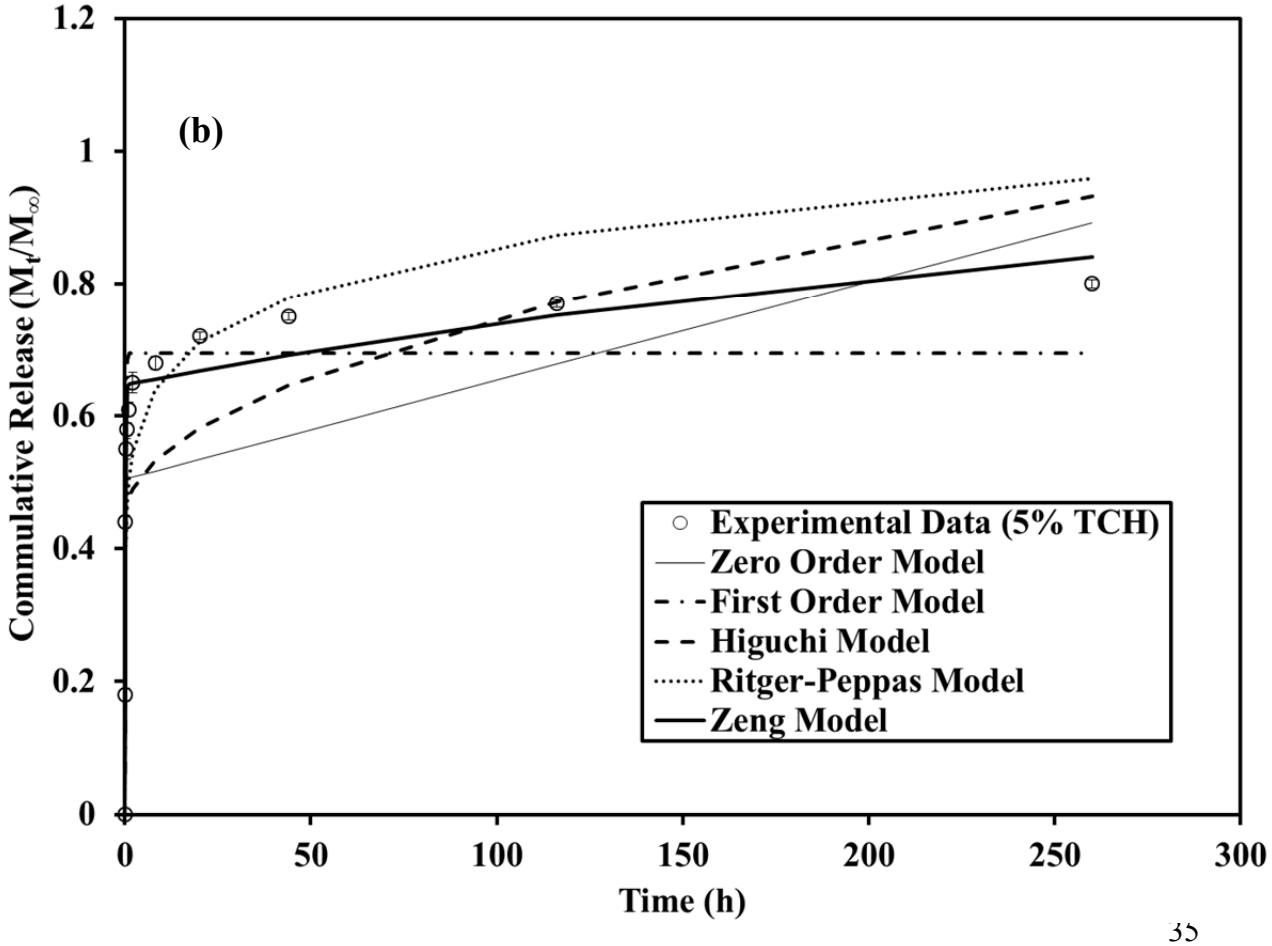
(b)
Commulative Release (M_t/M_∞)
Time (h)
Experimental Data (5% TCH)
Zero Order Model
First Order Model
Higuchi Model
Ritger-Peppas Model
Zeng Model

Fig. 8

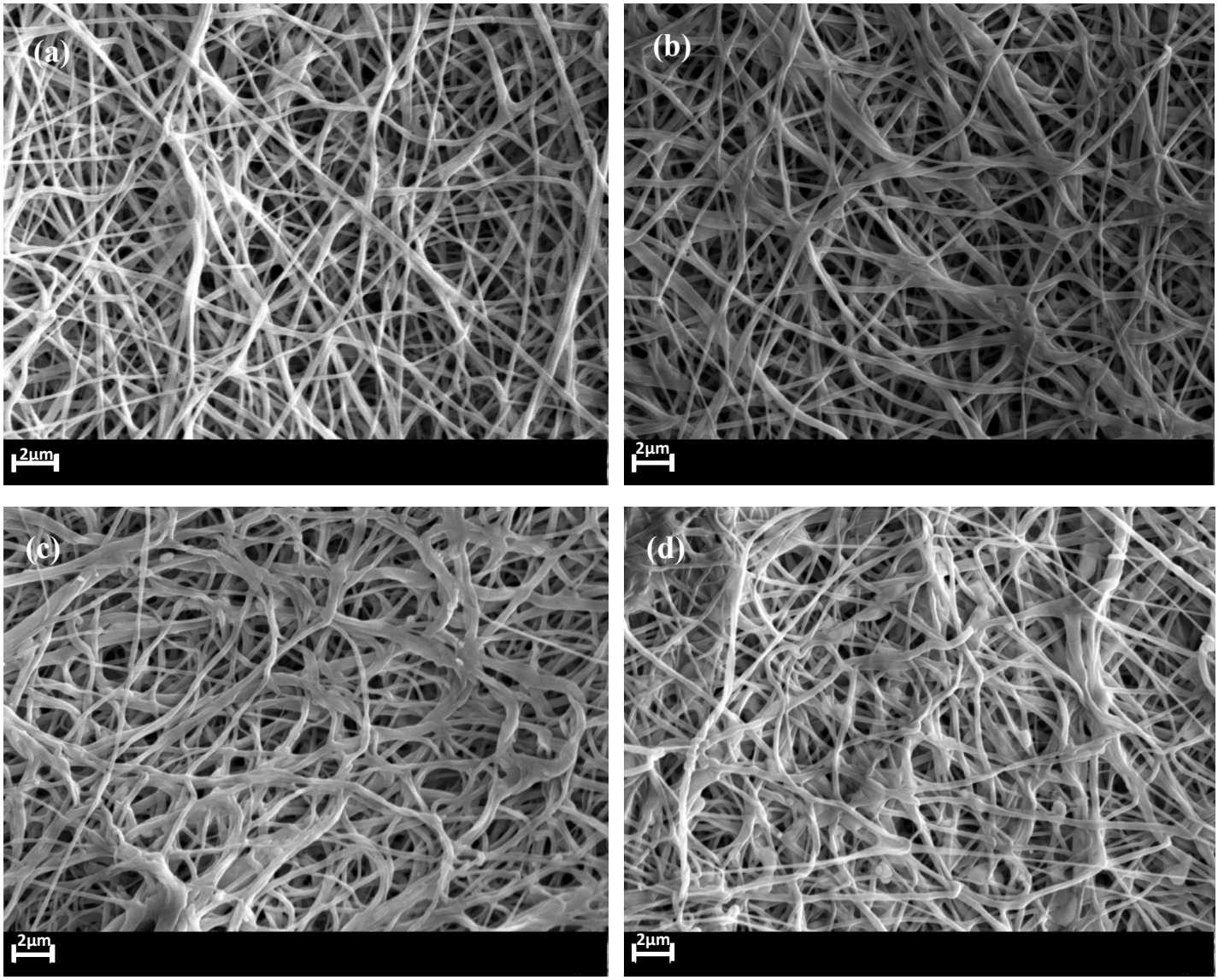

Fig. 9

Table 1 Effect of TCH concentration on the electrical conductivity of PLA: PCL (1:1) solutions

TCH concentration (wt%)	Electrical conductivity (μS/cm)	SD*
0	1	0.10
1	31	1.05
5	90	1.32

*SD= standard deviation

Table 2 DSC results* for electrospun PLA fibres, PCL fibres and PLA: PCL fibres loaded with or without TCH

Material sample	T_g (°C) PCL	T_m (°C) PCL	T_g(°C) PLA	T_c (°C) PLA	T_m (°C) PLA	Xc (%)**
PLA (Fibres)			64.1	87.20	155.60	12.6
PCL (Fibres)	-60.30	63.3				67.7
PLA: PCL (3:1)	–59.72	60.54		81.27	151.70	36.65
PLA : PCL (1:1)	–56.15	62.20		81.13	151.59	46.11
PLA: PCL (1:1)/ (1%TCH)	–58.38	60.35		80.42	151.55	45.04
PLA: PCL (1:1)/ (5%TCH)	–60.51	60.61		99.27	151.02	43.02

*Calculations were repeated for three sets of samples. The standard deviation for the T_g, T_c and T_m values was less than 0.5°C.

** Calculate from XRD data.

Table 3 Parameters obtained by fitting five different models to the release data for drug release kinetics

Model type	PLA: PCL (1:1) /(1% TCH)	PLA: PCL (1:1) /(5% TCH)
Zero order model	K_0=0.0017 R^2=0.291	K_0=0.0015 R^2=0.224
First order model	K_1=3.372 R^2=0.889	K_1=6.899 R^2=0.930
Higuchi model	K_H=0.035 R^2=0.489	K_H=0.030 R^2=0.387
Ritger-Peppas model	K_R=0.912 n=0.167 R^2=0.779	K_R=0.692 n=0.117 R^2=0.828
Zeng model	K_{on}=0.0025 h^{-1} K_{off}=0.0036 h^{-1} K_s=5.127 h^{-1} ΔG=1.47×10^{-21}J R^2=0.948	K_{on} =0.0017 h^{-1} K_{off}=0.0031 h^{-1} K_s=8.343 h^{-1} ΔG=2.49×10^{-21}J R^2=0.975

Table 4 Mass loss of PLA: PCL (1:1) / (5% TCH) nanofibre mats during the degradation time

Degradation time (h)	3	12	24	72	168	336
Mass loss (%)	0.41	0.81	1.32	3.15	5.14	6.30
SD* (%)	0.036	0.110	0.176	0.170	0.153	0.2

*SD= standard deviation